Journal of Alloys and Compounds 517 (2012) 98–102

Contents lists available at SciVerse ScienceDirect

Journal of Alloys and Compounds

journal homepage: www.elsevier.com/locate/jallcom

The enhanced nucleation factors and field electron emission property of diamond synthesized by RF-PECVD

Guangmin Yang[a], Qiang Xu[b], Xin Wang[c], Weitao Zheng[c,*]

[a] College of Physics, Changchun Normal University, Jilin Province, Changchun 130032, PR China
[b] Changchun Institute of Technology, Changchun 130021, PR China
[c] Department of Materials Science, Key Laboratory of Mobile Materials, MOE, and State Key Laboratory of Superhard Materials, Jilin University, Changchun 130012, PR China

ARTICLE INFO

Article history:
Received 26 June 2011
Received in revised form 2 December 2011
Accepted 11 December 2011
Available online 19 December 2011

Keywords:
Diamond
Films
PECVD
Field electron emission property

ABSTRACT

In this work, submicron-diamond (SD), microcrystalline diamond (MD), and nanocrystalline diamond (ND) were synthesized using different substrates and pretreatment methods. In order to investigate influencing factors on nucleation, three techniques have been developed to create some density of diamond on substrate surfaces: (a) with chemical-etching technique (NaOH water solution at 80 °C for 3, 8, 15 min, respectively), (b) $Co(NO_3)_3/Mg(NO_3)_2{\cdot}6H_2O$ or $Fe(NO_3)_3{\cdot}9H_2O/Mg(NO_3)_2{\cdot}6H_2O$ alcohol solution) dripping on silicon substrate, and (c) NaCl substrate directly by following a same PECVD deposition procedure. Furthermore, the field electron emission property was also investigated.

1. Introduction

The CVD diamond films offer unprecedented advantages as field emitter material over the other semiconducting materials due to their unique physical and chemical properties [1]. As the diamond grain size is reduced to nanoscale, the conducting pathway formed by graphite in the crystal boundaries is enhanced by hundreds of times, which greatly increases the film conductivity [2]. Furthermore, ND films have nanoscale smooth surfaces for convenient applications. In contrast, carbon nanotube (CNT) films, although possess superior field electron emission properties to the diamond films, have short lifetimes and poor emission stability [3]. Therefore, there are wide interests in improving the field electron emission properties of diamond films recently. One of the possible routes for increasing the field electron emission capacity of diamond films is to increase the proportion of grain boundary region, as it has been proposed that the grain boundaries contain sp^2-bonded carbon and provide conduction path for electron, which facilitates the field electron emission process. Accordingly, several similar field electron emission mechanisms have been proposed for diamond films [4–6]. Increasing nucleation density and content of sp^2 phase of grain boundary is of critical importance for synthesizing ND and improving the field electron emission property. The initial nucleation density and the nucleation rate during the growth affect the morphology and the microstructure of the thin films. And the morphology and the microstructure have great influence on the films' field emission property [7]. Recently, various techniques have been applied to enhance the nucleation rate for growing diamond films in CH_4—H_2 plasma. Scratching, ultrasonication and negative biasing (or biased enhanced nucleation) are three major surface pretreatment techniques that are widely used to create and enhance nucleation sites for diamond growth [8–10]. In this work, we synthesized diamond with different sizes and nucleation densities, using two kinds of substrate pretreatment methods with different substrates, and explored the field electron emission property for diamond films.

2. Experimental

The n-type Si (1 0 0) substrates were cleaned ultrasonically in acetone, alcohol and de-ionized water for 10 min consecutively prior to pretreatment. Diamond with different grain scales was synthesized using RF-PECVD via different substrate and pretreatment methods. Prior to deposition for submicron-diamond (SD) and micron-diamond (MD) films, NaOH water solution was used to roughen the silicon surface for 3, 8 and 15 min, respectively, while for uniformly dispersed ND particles or ND films, $Co(NO_3)_3/Mg(NO_3)_2{\cdot}6H_2O$ or $Fe(NO_3)_3{\cdot}9H_2O/Mg(NO_3)_2{\cdot}6H_2O$ alcohol solution was dripped on the silicon substrate prior to deposition. NaCl (1 0 0) substrate was also selected to deposit nanodiamond films. The RF-PECVD chamber was pumped down to 10 Pa by a rotary pump, and then pure hydrogen (99.99%) with a constant flow rate of 80 sccm was introduced into the chamber and the pressure was maintained at 1200 Pa. The substrate was heated to 800 °C in 40 min and pure methane (99.99%) with a flow rate of 15 sccm was introduced into the chamber for the growth of SD, MD, and ND films. During the growth process, a radio frequency power of 260 W was applied and the substrate temperature was kept at 800 °C. After 40 min deposition, CH_4 inlet was shut off and the system was allowed to cool down

* Corresponding author. Fax: +86 431 85168246.
E-mail address: wtzheng@jlu.edu.cn (W. Zheng).

0925-8388/$ – see front matter © 2011 Elsevier B.V. All rights reserved.
doi:10.1016/j.jallcom.2011.12.032

Table 1
The pre-treatment and deposition conditions of samples (1)–(5), where etching denotes NaOH water solution etching silicon substrates, metal denotes $Mg(NO_3)_2/Fe(NO_3)_3$ alcohol solution dropped on Si substrate, T temperature (°C), P deposition pressure (Pa), deposition time (40 min), and CH_4/H_2 (sccm).

Sample	Substrate	Pre-treatment	T	P	CH_4/H_2	Size	Products
(1)	Si	–	800	1200	15/80	–	–
(2)	Si	Etching	800	1200	15/80	8 μm	MD films
(3)	Si	Metal	800	1200	15/80	15 nm	ND films
(4)	NaCl	–	800	1200	15/80	20 nm	ND films
(5)	Si	Metal	800	1200	80/20	–	CNTs

to room temperature. The detailed experimental parameters are listed in Table 1. The obtained films were characterized by SEM (JOEL JSM-6700F), HRTEM (JOEL JEM-2010 at 300 kV), Raman spectroscopy (JOBINYVON HR800 with 632 nm excitation wavelength) and field emission measurement.

3. Results and discussion

Fig. 1(a)–(c) is the SEM image for the SD, MD films grown on silicon substrate with alkaline etching process, from which the diameter of the diamond particles is in the range of 1–8 μm. Increasing etching time, the silicon surface becomes rougher, and more deep pits form, hence the grain scales of the diamond grow larger with the same deposition time. In contrast, ND particles appear when only $Co(NO_3)_3/Mg(NO_3)_2$ alcohol solution is dripped on the silicon substrate. Interestingly, the ND particles on silicon surface are uniformly dispersed (Fig. 1(d)). When the $Fe(NO_3)_3{\cdot}9H_2O/Mg(NO_3)_2{\cdot}6H_2O$ alcohol concentration is higher compared to $Co(NO_3)_3/Mg(NO_3)_2{\cdot}6H_2O$ alcohol solution, ND films with a high nucleation density is achieved (Fig. 1(e)).

Fig. 2 exhibits Raman spectra for ND films grown on NaCl substrate, ND particles, and ND films, in the range of 1000–2000 cm^{-1}. The first peak position for the ND films grown on NaCl substrate, ND particles and ND films locates at 1332 cm^{-1} [11]. This result accords well with what Filik has reported [12]. They have calculated the Raman spectra of diamond, and observed the variation of the spectra with molecular size using Hartree–Fock theory. No evidence for Raman active vibrations of diamond nanocrystals at either 1150 or 500 cm^{-1} is found, regardless of whether hydrogen is terminated or confined in a matrix. Their investigation for the first time demonstrates that it is not correct that 1150 cm^{-1} or 500 cm^{-1} is always suggested as an evidence for ND. They have emphasized that only the broadened zone-center (1332 cm^{-1}) mode can be used as the fingerprint for ND.

Fig. 3(a) shows a TEM image with a lower magnification for ND films from Fig. 1(e), wherein it can be seen that the size of the nanoparticles is about 15 nm. Fig. 3(b) and (c) is TEM image for the nanodiamond grown on NaCl substrate, and Fig. 3(d) is the magnified image corresponding to area denoted by arrow in Fig. 3(b), the spacing of the lattice fringes is about 0.21 nm, which accords well with that for the single crystalline diamond (1 1 1). Hence, the HRTEM images further show that the ND has been achieved on NaCl substrate. From high resolution TEM images – Fig. 3(e) a part of the shell near the edge and Fig. 3(f) inside for nanodiamond from the arrow area in Fig. 3(c), and from their lattice fringes, we can see that nanodiamond particles are embedded in graphite shell. We can see that HRTEM images accord well with the observation from Raman results.

It is well known that the nucleation density of diamond on almost all substrates is very low, which is a consequence of the high surface energy of diamond. Thus, for SD, MD before deposition, the alkaline etched-Si surface is obtained. Our opinion is that alkaline etched-Si surface merely creates a change in the surface morphology, such as edges, steps, pits, dislocations, and other surface defects. These kinds of defects are labeled chemical active

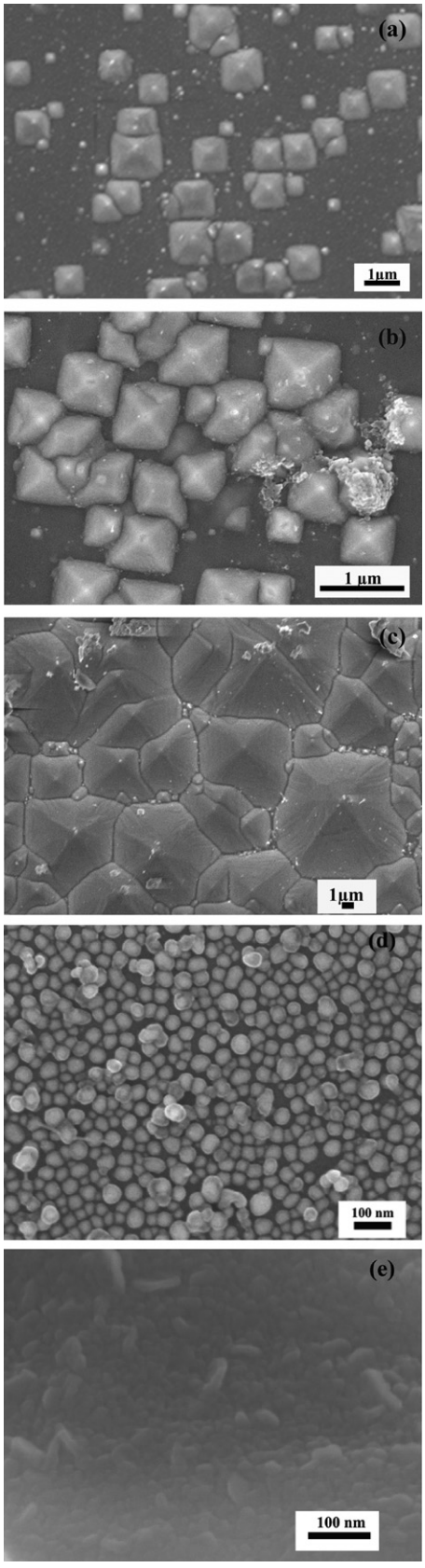

Fig. 1. SEM images for (a) SD, (b) SD, and (c) MD films with NaOH solution etching silicon substrates for 3, 8, and 15 min, respectively, (d) ND particles with $Co(NO_3)_3/Mg(NO_3)_2{\cdot}6H_2O$ alcohol solution dripping on the silicon substrate and (e) ND films with $Fe(NO_3)_3{\cdot}9H_2O/Mg(NO_3)_2{\cdot}6H_2O$ alcohol solution dripping on silicon substrate, before deposition.

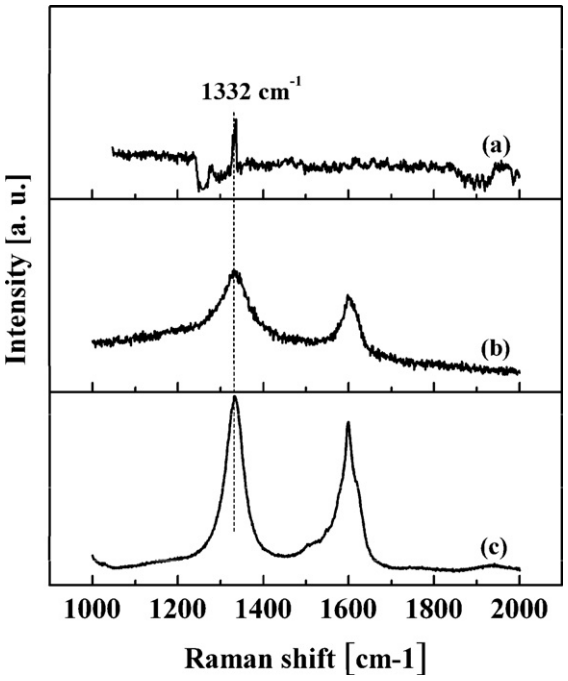

Fig. 2. Raman spectra for (a) ND films grown on NaCl substrate; (b) ND particles, and (c) ND films grown on silicon substrate.

sites, which prefer to adsorb diamond precursors together [13]. In this work, with increasing the etching time, the size of diamond enhances. As the microcosmic morphology of substrate can affect the nucleation energy around the interface, the nucleation energy is lower on the rough surface, diamond nucleates at the etching area easily and sp^3 forms predominance compared to sp^2, diamond grows up during deposition. It is difficult to form two-dimensional nucleation, when the diamond particles cover all the etching area, thus, diamond will stop growth.

However, as nanodiamond films deposit on NaCl substrate, the nucleation is easily formed without any pretreatment for substrate. This is probably due to that the NaCl substrate is quite rough, leading to decrease of diamond nucleation energy. Furthermore, the nanodiamond size is very uniform, as the NaCl surface has a uniform rough degree that does not like that of the alkaline etched-Si surface.

In conventional diamond growth method, one uses a highly dilute concentration of methane in hydrogen, the so-called hydrogen rich gas phase chemistry known to reduce re-nucleation by the significantly higher etch rate of graphite over diamond in such plasma [14]. Thus the suppression of re-nucleation results in an evolution of grain size from the small crystals at the seeded substrate to the film surface. For nanodiamond films, it is achieved by reducing the hydrogen concentration in the plasma to allow some sp^2 bonding to create new unepitaxial nucleation sites on the facets of growing crystals. Thus, there is a combination of epitaxial growth on these small crystals and the initiation of new crystals [11]. The constant interruption of the crystal evolution means that there is a fundamental limit on the maximum grain size and thus thick films can be grown with a small distribution of grain sizes. Some similar reports demonstrate that both ND and MD growth starts from individual nucleation sites. In the case of MD, well-faceted single crystallites are observed while in ND deposition, ballas- or cauliflower-like structures appear. The very difference between both cases is the rate of secondary nucleation, which is low for poly- but very high for nanocrystalline diamond film growth [15]. However, in this work, although SD, MD and ND grow in the same deposition conditions, they just do not start from individual nucleation sites, and we did not find the re-nucleation phenomenon in our HRTEM results.

Nucleation is the first and critical step of CVD diamond growth. The control of nucleation is essential for optimizing the diamond properties such as grain size, orientation, transparency, adhesion, and roughness that are necessary for targeted applications. In this paper, the nanodiamond nucleation density on the MgO-supported Co/Fe catalyst approaches several orders of magnitude higher than that on alkaline-etched pretreated Si wafers. It can be seen from Fig. 1 that the substrate MgO-supported Fe nanoparticles on Si substrate is covered with a dense ND film. No voids can be detected at the interfaces indicating that the nucleation density is very high. In fact, each point of the surface seems to serve as a nucleation site.

The reaction process for growing ND particles and films can be described as follows: firstly, MgO and CoO/Fe_2O_3 decompose from $Mg(NO_3)_2{\cdot}6H_2O$ and $Co(NO_3)_3/Fe(NO_3)_3{\cdot}9H_2O$, and then in the process of heating MgO and CoO/Fe_2O_3 at 800 °C in a H_2 atmosphere, CoO/Fe_2O_3 is reduced to Co/Fe by H_2. Here, MgO with good hydrophilicity and dispersion could be used to precisely control the particle size of Co/Fe [16], and hence Co/Fe particles can disperse well on the supported materials. In general, diamond is difficult to nucleate on the mirror-polished Si substrate, which is a consequence of its high surface energy ($3.7\,J\,m^{-2}$). We believe that Co/Fe particles play an important role in growing ND. On one hand, Co/Fe particles can offer the nucleation sites for diamond and reduce its nucleation energy [17]. On the other hand, Co/Fe particles effectively increase the possibility to adsorb carbon species, decomposed from gas precursor. The adsorbed carbon species accumulate on the surfaces of Co/Fe particles, and act as nucleation sites for diamond or graphite. Under the condition of discharging a H_2-rich mixture gas (H_2/CH_4), a large number of atomic hydrogen species appear, and they selectively etch the non-diamond carbon bonding such as sp^2 during growth. Only after a long incubation period, diamond can nucleate from the sites occupied by carbon species. However, since Co or Fe particles play a catalytic role in preferentially forming graphitic phase, as ND size increases, graphite appears, leading to that the ND particles are quickly wrapped by graphite. Therefore, ND cannot grow too large, and the diameter of ND is generally below 15 nm, while the nucleation density for ND depends on the number of the sites occupied by Co/Fe particles. However, if the $Ni(NO_3)_2{\cdot}6H_2O/Mg(NO_3)_2{\cdot}6H_2O$ or $Co(NO_3)_3/Mg(NO_3)_2{\cdot}6H_2O$ alcohol solution is also used prior to deposition, and a low gas flow rate ratio of H_2/CH_4 (20:80) is used during deposition, CNTs are mainly obtained. Thus, hydrogen plays a most decisive role in the deposition of diamond films for the gas phase and surface processes.

4. Field electron emission properties

Fig. 4 shows *J–E* profiles and Fowler–Nordheim (FN) plots of the field electron emissions from (⌒) MD, (●) ND particles, and (▲) ND films, respectively. As shown in Fig. 4(a), the turn-on fields corresponding to an electron emission density of $10\,\mu A/cm^2$ are 7, 3.2, $2\,V/\mu m$ for MD, ND particles, and ND films, respectively. As a result, the obtained ND films exhibit the superior field electron emission properties. Moreover, at the applied field of $7\,V/\mu m$, the ND films have the highest emission current density among the three samples. This may be caused by (1) more emission sites in ND films; (2) small grain size; and (3) the increase in the proportion of sp^2-bonded grain boundaries. The deviation from the straight lines and obvious fluctuations were observed for the F–N plots in the region of low electric field. This may be due to the effect of residual gas absorption and desorption on the sample surface. Using strong electric field, the residual gas molecules are removed and its effect is weakened [18]. The F–N plot becomes straight line. The

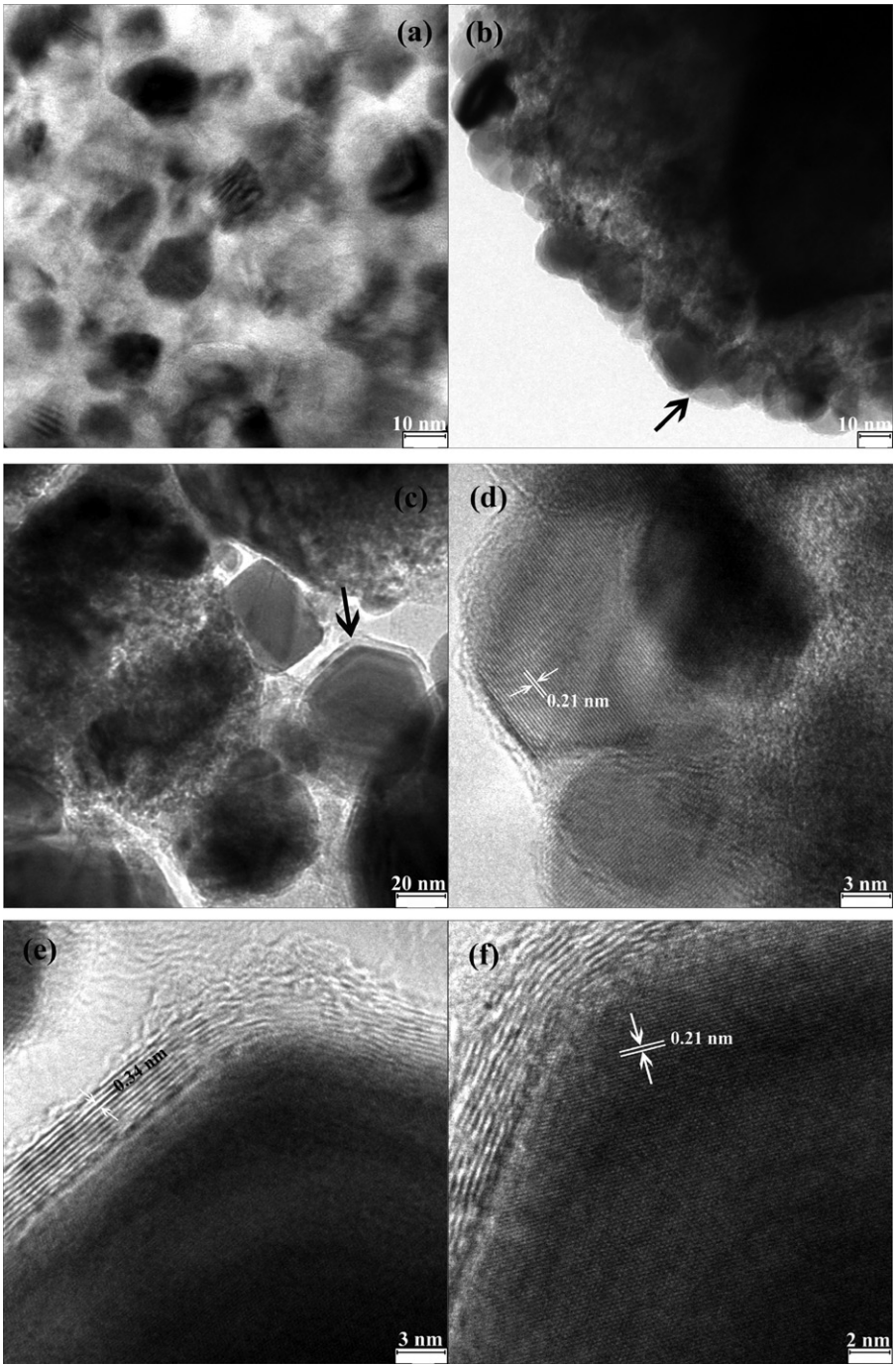

Fig. 3. (a) TEM images for ND films from Fig. 1(e); (b) and (c) TEM images for the ND films grown on NaCl substrate, and (d) the magnified images corresponding to arrows denoted in (b); high resolution TEM images (e) and (f) from (c) a part of the shell near the edge, and the inside for nanodiamond.

Fowler–Nordheim (FN) plots [$\ln(J/E^2)$ vs. $1/E$] for the above three samples in the region of strong electric field shown in Fig. 4(b) are in good agreement with the Fowler–Nordheim equation as follows: $\ln(J/E^2) = \ln(A\beta^2/\varphi) - B\varphi^{3/2}/\beta E$, where $A = 1.54 \times 10^{-6}$ A eV V^{-2}, $B = 6.83 \times 10^3$ eV$^{-3/2}$ V μm^{-1}, $\beta = (-B\varphi^{3/2}/S_{FN})$ is the field enhancement factor with S_{FN} being the slope of the FN plots, and φ is the work function of emitters. It is known that the work function depends mainly on the material. However, orientation of crystals may also affect the work function [19–21]. For diamond, work function values in the range of 4–5 eV have been used by other authors [22]. In this paper, a constant work function value of 4.5 eV has been assumed for all diamond with different scales investigated in this study. $\beta = 1.5 \times 10^3$, 4.8×10^3, and 7.8×10^3 can be obtained for MD, ND particles, and ND films, respectively ($\varphi_{diamond} = 4.5$ eV). It is evident that the β values of the ND particles are much higher than those of the MD. It is well known that the enhancement factor β can reflect the ability of the emitters to enhance the local electric field at the tip compared the average macroscopic value. The bigger the enhancement factor β, the better the field emission property for ND particles. Therefore, the field electron emission enhancement of ND particles can be attributed to an increase in the enhancement factor β due to the decrease of grain scale. In addition, the graphite as a conduction channel can enhance the transport of electrons from the substrates into the ND surface during field emission [23].

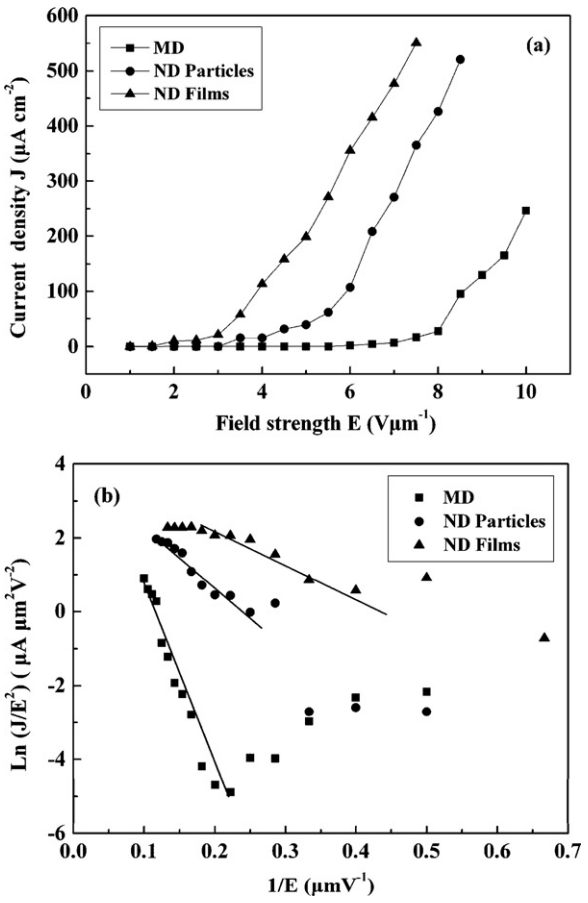

Fig. 4. Field emission current density as a function of electric field for (⌒) MD films, (●) ND particles, and (▲) ND films in (a). The Fowler–Nordheim (F–N) plots, corresponding to MD films, ND particles, and ND films, respectively in (b).

The field emission property of ND films, compared with ND particles, has been remarkably improved. Fig. 4(b) shows that there is no significant difference in the field enhancement β between the ND particles and ND films. Hence, the enhancement caused by geometry could be negligible in the present study. The grain density, scales and more sp^2 content are important factors to influence the emission behavior of the ND films. It has been reported that the more content of sp^2-bonded grain boundaries, the better field emission properties for ND films. Our results suggest that the formation of graphite decreases the interface barrier, improves the back contact between silicon and ND films, and can enhance the transport of electrons from the substrates into the ND surface as a conduction channel during field emission which is the dominant reason for the field emission enhancement of ND films.

5. Conclusions

Diamond nucleation was performed on the silicon substrate pretreated by two different methods and NaCl substrates, respectively. A drastic nucleation enhancement was obtained on the silicon substrates pretreated with Fe mixed MgO nanoparticles and NaCl substrate. It may thus be concluded that MgO, Fe particles and hydrogen play important roles in the formation of nanodiamond, and the density of primary nucleation is determined by macroscopic morphology of the substrates.

FEE properties of diamond with different grain scales have been characterized and investigated. The results demonstrate that the FEE properties of ND films markedly increase as the nucleation density increases, due to the formation of large proportion of grain boundaries. These findings indicate that the high-performance ND film with good field electron emission property is one of the most promising materials for cold-cathode electron sources.

Acknowledgements

The project is financially supported by Natural Science Foundation of Changchun Normal University, the National Natural Science Foundation of China (Grant Nos. 50525204, 50832001 and 51002061), the Fundamental Research Funds for the Jilin University (Grant No. 200903015), the Special Ph.D. program (Grant No. 200801830025) from MOE, the “211” and “985” project of Jilin University, China, the Science and Technology Development Programmer of Jilin Province (Grant No. 20090703), the Natural Science Foundation of Jilin Province (Grant No. 201115019), and the Program for Changjiang Scholars and Innovative Research Team in University.

References

[1] Y.C. Lee, S.J. Lin, C.T. Chia, H.F. Cheng, I.N. Lin, Diam. Relat. Mater. 13 (2004) 2100.
[2] D.M. Gruen, Annu. Rev. Mater. Sci. 29 (1999) 211.
[3] S.I. Cha, K.T. Kim, S.N. Arshad, C.B. Mo, K.H. Lee, S.H. Hong, Adv. Mater. 18 (2006) 553.
[4] J.E. Yater, A. Shih, J.E. Butler, P.E. Pehrsson, Appl. Surf. Sci. 191 (2002) 52.
[5] K.H. Wu, E.G. Wang, Z.X. Cao, Z.L. Wang, X. Jiang, J. Appl. Phys. 88 (2000) 2967.
[6] J.E. Yater, A. Shih, J.E. Butler, P.E. Pehrsson, J. Appl. Phys. 96 (2004) 446.
[7] M. Fhaner, H. Zhao, X. Bian, J.J. Galligan, G.M. Swain, Diam. Relat. Mater. 20 (2011) 75.
[8] F. Arezzo, N. Zaccheti, W. Zhu, J. Appl. Phys. 75 (1994) 5375.
[9] X. Jiang, W.J. Zhang, C.P. Klages, Phys. Rev. B 58 (1998) 7064.
[10] D. Pradhan, L.-J. Chen, Y.-C. Lee, C.-Y. Lee, N.-H. Tai, I.-N. Lin, Diam. Relat. Mater. 15 (2006) 1779.
[11] O.A. Williams, M. Nesladek, M. Daenen, S. Michaelson, A. Hoffman, E. Osawa, K. Haenen, R.B. Jackman, Diam. Relat. Mater. 17 (2008) 1080.
[12] J. Filik, J.N. Harvey, N.L. Alian, P.W. May, Phys. Rev. B 74 (2006) 035423–35431.
[13] S. Yugo, A. Izumi, T. Kanai, T. Muto, T. Kimura, Proc. of the 2nd Int. Conf. on New Diamond Science and Technology, Pittsburg, PA, MRS, 1991, p. 385.
[14] M. Frenklach, J. Appl. Phys. 65 (1989) 5142.
[15] W. Kulisch, C. Popov, Phys. Stat. Sol. (a) 203 (2006) 203.
[16] G.Q. Ning, Y. Liu, F. Wei, Q. Wen, G.H. Luo, J. Phys. Chem. C 111 (2007).
[17] W.D. Harkins, J. Chem. Phys. 10 (1942) 268.
[18] X. Lu, Q. Yang, C. Xiao, A. Hirose, Thin Solid Films 516 (2008) 4217.
[19] J. Van der Weide, R.J. Nemanich, Appl. Phys. Lett. 62 (1993) 1878.
[20] J. Van der Weide, R.J. Nemanich, J. Vac. Sci. Technol. B 10 (1992) 1940.
[21] J. Van der Weide, Z. Zhang, P.K. Baumann, M.G. Wensell, J. Bernholc, R.J. Nemanich, Phys. Rev. B 50 (1994) 5803.
[22] W.A. Mackie, J.E. Plumlee, A.E. Bell, J. Vac. Sci. Technol. B 14 (1996) 2041.
[23] J. Chen, S.Z. Deng, J. Chen, J.C. She, N.S. Xu, J. Appl. Phys. 94 (2003) 5429.